

Mössbauer study of 1% ^{57}Fe doped ferromagnetic insulator $\text{La}_{0.825}\text{Ca}_{0.175}\text{MnO}_3$

M. Pissas^{1,a}, G. Papavassiliou¹, E. Devlin¹, A. Simopoulos¹, and V. Likodimos²

¹ Institute of Materials Science, NCSR, Demokritos, 15310 Aghia Paraskevi, Athens, Greece

² Department of Physics, National Technical University of Athens, 157 80 Athens, Greece

Received 21 July 2004 / Received in final form 11 May 2005

Published online 11 October 2005 – © EDP Sciences, Società Italiana di Fisica, Springer-Verlag 2005

Abstract. We have employed magnetization measurements, Mössbauer and ESR spectroscopic techniques, in order to study the ferromagnetic insulating (FMI) compound $\text{La}_{1-x}\text{Ca}_x\text{MnO}_3$ ($x = 0.175$) doped with 1% ^{57}Fe . We have used two samples; one prepared in air which has cation vacancies and a second in inert atmosphere, which is stoichiometric. An abrupt change of the experimental results is obtained, by all techniques, in the ferromagnetic insulating regime, in the temperature region of $T_{O/O//} \approx 60$ K, where an orbital rearrangement is suggested to occur. An analysis of these findings points to an orbital rearrangement transformation. Ferromagnetic resonance reveals considerable differences between stoichiometric and cation deficient samples, indicating anisotropy of the exchange interactions in the former sample with significant temperature dependence, most pronounced in the vicinity of $T_{O/O//}$

PACS. 87.64.Pj Mössbauer spectroscopy – 75.47.Lx Manganites – 75.50.Dd Nonmetallic ferromagnetic materials – 87.64.Hd EPR and NMR spectroscopy

1 Introduction

Despite the large number of works dedicated to the study of $\text{La}_{1-x}\text{Ca}_x\text{MnO}_3$ (see [1], and references therein) detailed elucidation of its ground state for certain values of x , is still an unresolved problem. The two end-compounds $x = 0$ and $x = 1$ are A and G-type antiferromagnets, respectively. As Ca substitutes for La in the LaMnO_3 compound, for $0 \leq x \leq 0.125$ the samples display an insulated canted antiferromagnetic (CAF) ground state, changing to ferromagnetic insulating (FMI) for $0.125 \leq x \leq 0.23$ and ferromagnetic metallic (FMM) for $0.23 \leq x < 0.5$. [2–4]

Although the FMM state has been explained partially by the double exchange model, the FMI state lacks a complete microscopic explanation. Ferromagnetic exchange interactions in insulating compounds, according to the Goodenough-Kanamori-Anderson rules, traditionally exist only for certain orbital orientations of Mn^{+3} orbitals in the perovskite structure. The experimental elucidation of the orbital ordering is not a simple task. Only indirectly can one detect the orbital ordering, through a particular ordering of the bond lengths in the crystal structure or by resonant X-ray scattering data at the manganese K edge. [5] For the $\text{La}_{1-x}\text{Ca}_x\text{MnO}_3$ and $\text{La}_{1-x}\text{Sr}_x\text{MnO}_3$ compounds, in the FMI regime, the crystallographic data are not clear enough to support any particular orbital

ordering which would explain, without any doubt, the orbital ordering driven ferromagnetic exchange interactions. Stoichiometric $\text{La}_{1-x}\text{Ca}_x\text{MnO}_3$ samples in the FMI regime, firstly undergo a structural transition at T_{JT} , from an orbital disordered state, to a cooperative Jahn-Teller orbital ordered state. In this orbital ordered state the orthorhombic splitting $s = 2(a - b)/(a + c)$ (a , b and c are the unit cell parameters) increases as the temperature decreases. On further cooling, a paramagnetic to ferromagnetic transition takes place at $T_c < T_{JT}$. Below T_c the orthorhombic strain parameter s decreases and at $T_{O/O//} \approx 60$ K the strain parameter becomes nearly temperature independent. [4,6] Nevertheless, although the crystallographic data, in the temperature regime $T_{O/O//} < T < T_c$, to a first approximation support the orbital ordering explanation of the FMI state, the structural transition at $T_{O/O//}$ further complicates the situation. This structural transition in the FMI regime reduces the orbital ordering driven ferromagnetic exchange interactions. In addition, the situation is further complicated since the FMI state also exists in samples with cation non-stoichiometry, which do not show a clear long range orbital ordered crystal structure. Samples prepared in air or in high oxygen partial pressure atmosphere are non-stoichiometric through cation vacancies [2,3,6] which are created at both La and Mn sites.

^a e-mail: mpissas@ims.demokritos.gr

In the case of $\text{La}_{1-x}\text{Sr}_x\text{MnO}_3$ let us review the data of the compound with $x = 1/8$ where detailed experimental results exist ([7] and references therein). This sample first undergoes a structural transition at $T_{\text{JT}} = 270$ K, from an orbital disordered state to a cooperative Jahn-Teller orbital ordered state. At $T_c = 185$ K, where the orthorhombic strain s becomes a maximum, a ferromagnetic transition takes place similar to the behavior of the $\text{La}_{1-x}\text{Ca}_x\text{MnO}_3$ compound. Subsequently, at $T_{\text{O/O}} = 150$ K a second structural transition occurs which is accompanied by a sudden drop of the orthorhombic strain and a step-like increase of the ferromagnetic moment. Based on the recent X-ray resonant scattering data, Geck et al. [7] proposed that the transition $T_{\text{O/O}} = 150$ K (which is the subject of the present article) concerns a static structural modulation phenomenon that reduces the orthorhombicity, increases the ferromagnetic moment, localizes the charge carriers and reduces the Jahn-Teller cooperative ordering (without completely canceling it). Geck et al. [7] called this complicated change an orbital rearrangement. In spite of state of the art measurements, it is not possible to draw a final answer for the ground state of the ferromagnetic insulating regime.

All the above unexplained features ask for a microscopic explanation. Besides scattering techniques which provide information on the average structure, probing a coherent volume, local experimental techniques may help to probe the system at the atomic level. The Mössbauer technique is a valuable tool since it gives information on the immediate neighborhood of the ^{57}Fe probe. The Fe^{3+} ion substitutes for Mn^{3+} without significant disturbance of the lattice, due to their similar ionic radii. The ESR technique (or FMR in the ferromagnetic regime) on the other hand, is extremely sensitive to changes of the magnetic anisotropy providing information related to the magnetic structure. In the field of manganese perovskites Mössbauer spectroscopy in low ^{57}Fe and ^{119}Sn -doped samples [8–16] has contributed useful information. As an example, the sublattice magnetization can be determined directly from the hyperfine field. We have investigated the FMI regime for $x = 0.175$ (i.e. the middle of the regime) with emphasis on the microscopic origin of the intricate behavior near the $T_{\text{O/O}}$ temperature. To this end we used samples prepared in air and inert atmosphere in order to clarify the role of non-stoichiometry. The analysis of the results points to an orbital rearrangement at $T_{\text{O/O}}$.

2 Experimental details

A sample with nominal composition $\text{La}_{1-x}\text{Ca}_x\text{Mn}_{0.99}\text{Fe}_{0.01}\text{O}_3$ ($x = 0.175$) was prepared by the standard solid state reaction method using Fe_2O_3 90% enriched with ^{57}Fe . We prepared two samples. The first sample was prepared in an air atmosphere in all stages of the preparation. We call this sample the Air Prepared sample (AP). The second sample was annealed in the final stage of the preparation at 1000 °C in an inert atmosphere and we call this the Reduced sample (R). The X-ray diffraction data at $T = 300$ K were analyzed using the Ri-

etveld refinement method (assuming the orthorhombic $Pnma$ space group for both samples) and revealed single phase materials. The lattice parameters for the AP and R samples were determined to be $a = 5.4883(1)$ Å, $b = 7.7585(2)$ Å, $c = 5.5062(1)$ Å and $a = 5.5012(4)$ Å, $b = 7.7706(4)$ Å and $c = 5.5093(4)$ Å, respectively. The R samples in this doping regime follow the so called O/structure ($a \gg c > b/\sqrt{2}$) for $T < T_{\text{JT}} \approx 270$ K [6]. On the other hand the AP sample adopts the O* structure ($c > a > b/\sqrt{2}$) [3]. In the temperature region 50–100 K, where a magnetic anomaly exists in the magnetic measurements in both R and AP samples, a reduction of the orthorhombic strain $s = 2(a-c)/(a+c)$ has been observed only in the R sample [6]. The absorption Mössbauer spectra (MS) were recorded using a conventional constant acceleration spectrometer with a $^{57}\text{Co}(\text{Rh})$ source moving at room temperature, while the absorber was kept fixed in a variable temperature cryostat equipped with a 6.5T superconducting magnet with the field perpendicular to the γ -rays. The resolution was determined to be $\Gamma/2 = 0.12$ mm/sec using a thin α -Fe foil. DC magnetization measurements were performed in a SQUID magnetometer (Quantum Design).

ESR experiments were carried out on a Bruker ER 200D spectrometer at the X-band ($\nu \approx 9.41$ GHz) with 100 kHz field modulation. The magnetic field was scaled with a NMR gaussmeter, while temperature dependent measurements were carried out in the range of 4–300 K employing an Oxford flow cryostat during heating runs. Measurements were performed using fine powdered samples dispersed in high vacuum grease or small ceramic pieces (mass of 1–2 mg).

3 Magnetic moment measurements

Figure 1a shows the temperature dependence of the dc magnetic moment (m) in a field of 100 Oe for the AP and R samples respectively measured using the SQUID magnetometer. For both samples the data were collected on heating (zero field cooling branch ZFC) and on cooling (field cooling branch FC). Both measurements show a sharp ferromagnetic transition at 180 K and 190 K for the R and AP samples respectively. In addition, strong irreversibility between ZFC and FC branch has been observed for both samples at a temperature (T_{irr}), slightly below T_c (see Fig. 1a). The ZFC branch displays a step-like increase within the temperature intervals $70 \leq T \leq 110$ K and $T_{\text{O/O}} = 70 \leq T \leq 90$ K for the AP and R samples respectively. The corresponding FC branches show a slope change at the upper limit of the temperature intervals mentioned above. Figure 1b shows the temperature variation of the real part of the ac susceptibility $\chi(T)$ for both samples. For the AP sample χ shows a temperature dependence characteristic of all the AP samples with $0 \leq x \leq 0.22$ (see [3]). In the interval $70 \leq T \leq 110$ K χ shows a similar temperature behavior to the corresponding ZFC branch of the dc magnetic measurements. The $\chi(T)$ curve for the R sample displays a narrow peak at

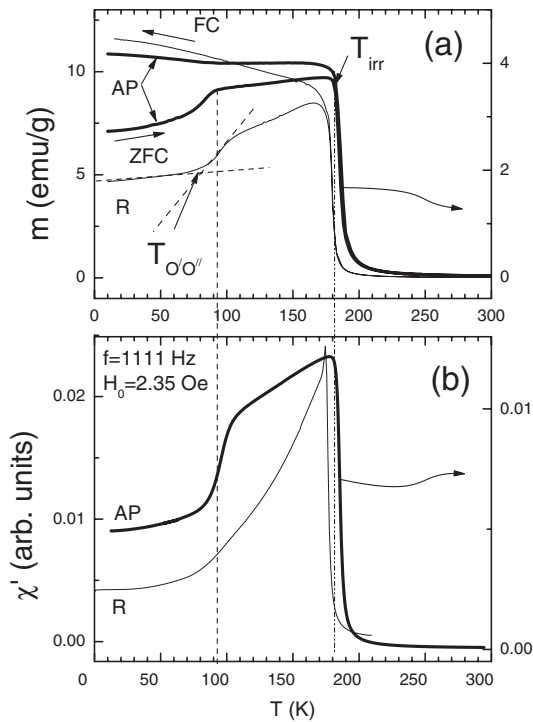


Fig. 1. (a) Temperature dependence of the magnetic moment at $H = 100$ Oe and (b) ac susceptibility of AP and R samples.

T_{irr} which is related to the Hopkinson effect [3] which signals the sudden drop of the anisotropy near T_c . We note that this particular behavior is observed only in R samples. The AP samples do not show such a peak, probably due to the isotropic character of the exchange interactions. As the temperature is reduced further there is a shoulder at 100 K. For $T < 60$ K $\chi(T)$ approaches $T = 0$ K with zero slope.

The irreversibility of $m(T)$ for $T < T_{\text{irr}}$ is sometimes an indication of spin glass behavior. This behavior however can also be attributed to domain wall pinning. Simply, the T_{irr} represents the temperature where pinning of the domain wall gives rise to a finite coercivity. Similarly, one could also invoke a mechanism that increases the cohesive field to interpret the abrupt change that occurs at ~ 60 K [17,18]. Some other researchers have attributed this feature to a spin glass behavior due to the observed frequency dependence in the particular temperature regime [19,20].

Figure 2 depicts the temperature variation of the electrical resistivity for the AP and R samples. The resistance of the AP sample displays a small peak at T_c indicative of a metal to insulator transition. A few degrees lower, the resistivity increases again as the temperature decreases. It is interesting that a small anomaly at $T_{O'O'}$ is also present in the resistance data. As far as the R sample is concerned, the resistance increases as the temperature decreases. In the semi-logarithmic plot we can recognize distinct anomalies corresponding to T_{JT} , T_c and $T_{O'O'}$.

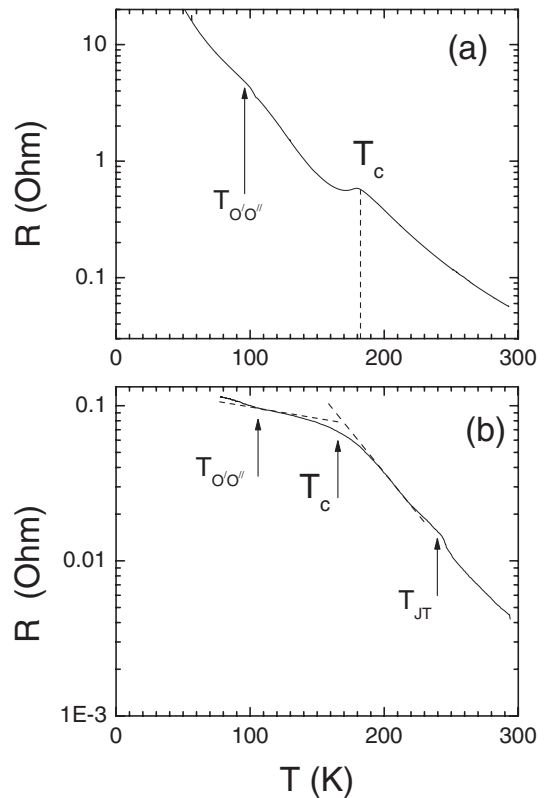


Fig. 2. Temperature variation of the electrical resistance of the AP (a) and R (b) samples.

4 Mössbauer spectra

Figures 3 and 4 show the temperature variation of the Mössbauer spectra of the AP and R samples respectively. At $T = 300$ K the spectra for both samples display a peak which can be fitted by an unresolved doublet, keeping the linewidth constant at the value found from the calibration. The isomer shift $\delta = 0.37$ mm/s is characteristic of high spin iron Fe^{+3} in an octahedral environment. The small value of the quadrupole splitting $\epsilon = 0.08$ mm/s indicates that for this particular x the crystal structure at $T = 300$ K does not display cooperative Jahn-Teller distortion, i.e. the MnO_6 octahedra are nearly undistorted and are rotated with respect to the ideal perovskite structure. It is interesting to note that similar values for ϵ were found for $x = 0.25$ and 0.33 compounds [8,13]. As the temperature passes the Curie temperature the spectra become magnetically split. Near T_c the spectra are rather complicated consisting of a distribution of hyperfine fields and a paramagnetic component. By further cooling, the paramagnetic component gradually disappears, and the width of the hyperfine field distribution decreases.

At $T = 4.2$ K, only one sextet is present with hyperfine parameters $H_{hf} = 526(1)$ kOe, $\delta = 0.506(2)$ mm/s, $\epsilon = 0.038(2)$ mm/s, and $(H_{hf} = 530(1)$ kOe, $\delta = 0.506(2)$ mm/s, $\epsilon = 0.023(1)$ mm/s), for the R and AP samples respectively. These hyperfine parameters are common for Fe^{+3} in an octahedral coordination and in the high spin state $S = 5/2$. Spectra taken at intermediate

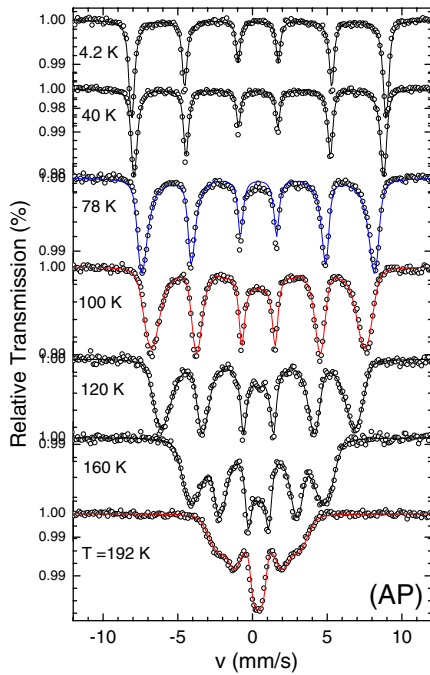


Fig. 3. Mössbauer spectra of (AP) sample. The solid lines through the experimental points results from a least-squares fit using the Le Caer-Dubois program.

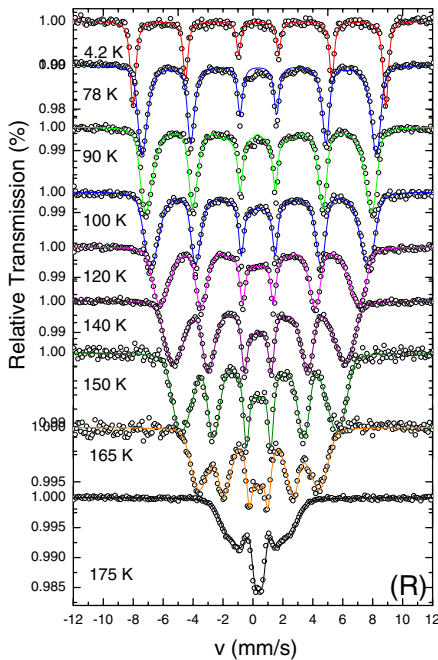


Fig. 4. Mössbauer spectra of (R) sample. The solid lines through the experimental points results from a least-squares fit using the Le Caer-Dubois program.

temperatures, were fitted by employing the Le Caer-Dubois program [21]. In this program a continuous distribution of magnetic components is assumed. The quadrupole interaction and the linewidth are the same for each component and only the magnetic hyperfine field varies in a continuous fashion. The resulting hyperfine field distributions $p(H)$ for both samples are depicted in Fig-

ure 5. The solid lines through the solid squares in the insets of Figure 5 are obtained from the mean-field approximation, by solving the equation $\sigma = B_J[(3J)/(J+1)(\sigma/\tau)]$, where $\sigma = H_{hf}(T)/H_{hf}(0)$ is the effective hyperfine field, $\tau = T/T_c$ is the reduced temperature, J is the spin of Fe in the high spin state ($J = 5/2$) and B_J is the Brillouin function [22]. The good agreement between the mean field approximation and the most probable hyperfine magnetic field means that the latter represents the host magnetic moment.

At $T = 4.2$ K, the $p(H)$ of the R sample is centered at about 525 kOe with a FWHM $\Delta \sim 15$ kOe. The same broadening is present up to 60 K (inset of Fig. 5). For $T > 60$ K the FWHM of the $p(H)$ increases linearly with temperature, up to T_c . Similar behavior is seen in the AP sample (Fig. 5) Interestingly, in order to account for the region of the spectrum near $v = 0$ it is necessary that the $p(H)$ be extended down to $H = 0$. This part of the $p(H)$ is more pronounced as T_c is approached. Clearly, the temperature variation of ΔH resembles the ZFC branch of the dc-magnetic moment or the real part of χ . If we accept a scenario that for $T < T_{O/O//}$ an orbital rearrangement occurs inside the FI phase, then the abrupt increase of ΔH presumably originates from the orbital degree of freedom for $T > T_{O/O//}$. At this point we note that the temperature variation of ΔH is different than that observed for the samples in the metallic regime $0.23 < x < 0.5$ [13–15]. In these cases $p(H)$ shows a tail in the low field part and as the temperature increases this tail spreads out to lower fields. In the $x = 0.175$ case the main peak broadens but in a symmetric fashion. The broadening ΔH can arise from various factors including chemical inhomogeneity, spin fluctuations, orbital fluctuations and spin-cluster fluctuations (superparamagnetism). Chemical inhomogeneity is temperature independent and should be excluded. Superparamagnetism is also excluded since in this case a paramagnetic peak should appear which increases with temperature. Spin fluctuations can arise from spin-lattice relaxation with a relaxation rate increasing with temperature, but an abrupt increase is not expected through this mechanism.

Mössbauer spectroscopy, in the ferromagnetic state, measures the hyperfine field $H_{hf}(T)$ via the line splitting which probes the spontaneous magnetization $M(T)$ of the ferromagnetic phase at the iron sites. For a typical isotropic ferromagnet, such as α -Fe, the MS below the critical temperature consist of a sextet with narrow Lorentzian lines. As the temperature increases from zero, the Zeeman splitting decreases while the line width remains constant up to the critical regime. Line broadening due to collective excitation spin waves is unobserved because the fluctuations of \mathbf{S} with respect to S , in such a case are so fast in comparison with a Larmor frequency at a field of 200 kOe ($f_L \sim 5 \times 10^9$ Hz) that they average out. This is true in normal ferromagnets where the bottom of the spin wave branch is higher than the Mössbauer frequencies except in the immediate vicinity of T_c , where very small critical effects have been observed. Based on the above discussion and data from neutron studies of

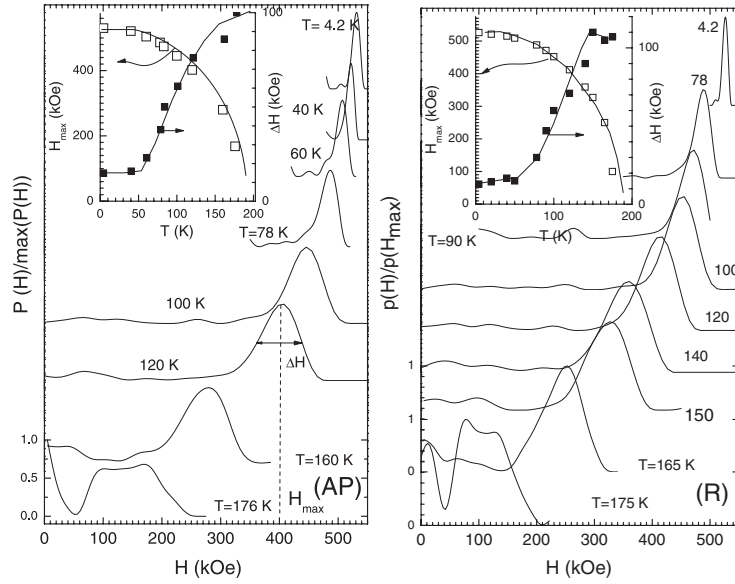


Fig. 5. Temperature dependence of the distribution $p(H)$ of the magnetic hyperfine field of for AP (left panel) and R (right panel) samples, estimated from a least-squares fit using the Le Caer-Dubois program. The insets in the corresponding panels display the temperature variation of the maximum value of the hyperfine field distribution (open squares) and the width of the distribution (solid squares). The solid lines through the open squares represent mean-field solutions of the equation $\sigma = B_J[(3J)/(J+1)(\sigma/\tau)]$. The solid lines through the solid squares are guides to eye.

the pristine sample [6], the observed increasing of the inhomogeneous broadening is most probably related to the structural transition occurring at $T_{O/O//}$ (see below).

We turn now to the microscopic origin of the hyperfine field distribution as revealed in MS. In ferric oxides, contributions to H_{hf} from orbital angular momentum and conduction-electron polarization are rigorously absent, while those from dipolar sources are small. This leaves only the contact field, which is proportional to the net polarization of the s -electron density at the nucleus in question. The contact field (H_{con}) is the vector sum of a local part H_{loc} and a supertransferred part H_{ST} . H_{loc} is proportional to the local $3d$ spin S_0 on the ion ($S = 5/2$ for the case of Fe^{+3}) while H_{ST} is the magnetic field at a nucleus generated by the spin at a neighbor site (\mathbf{S}_n) by transfer and overlap effects through the intervening anion. The resulting field is:

$$\mathbf{H}_{hf} \approx H_{con} = -C(\mathbf{S}_0/S) + \sum_n B_n(\mathbf{S}_n/S) \quad (1)$$

where C and B_n are positive scalar parameters [23]. The B_n parameters are associated with the coordination geometry and can be expressed as a function of the Fe-O-Fe or Fe-O-Mn bond angle ϕ_n , namely $B_n = H_\pi + (H_\sigma - H_\pi) \cos^2 \phi_n$. In this equation the fields $H_{\pi,\sigma}$ arise from overlap distortions of the Fe cation s orbitals caused by the ligand p orbitals having been unpaired by spin transfer via π and σ bonds into unoccupied $3d$ orbitals on the NN cations n . We propose here that the linewidth of the distribution $p(H)$ and its temperature dependence, arises from the transferred part of the hyperfine interactions. The linewidth up to 60 K is small and constant and it represents mainly inhomogeneities in the sample. Above this temperature its abrupt increase displays fluctuations of the transferred hyperfine field arising

from the orbital disorder. In our case $H_{loc} + H_{ST} = -530$ kOe (the minus sign means that H_{hf} is antiparallel to the iron spin). By virtue of theoretical calculations [23] it has been deduced that $H_{loc} = -450$ kOe in octahedral oxygen coordinated ferric iron, a fact implying that the iron moment must be antiferromagnetically coupled with the six nearest-neighbor manganese ions. This antiferromagnetic coupling is experimentally verified by taking spectra in the presence of an external field (vide infra).

Summarizing here, we argue that the abrupt increase of the width of the hyperfine field distribution in the R sample is related to fluctuations of the supertransferred field. We speculate that these fluctuations are related to the different orbital state that exists below $T_{O/O//}$. Above $T_{O/O//}$ the manganese e_g orbitals, although on average preserving some characteristics of orbital ordering observed in LaMnO_3 , also possess a fluctuating component which produces significant fluctuations in the supertransferred field. It is interesting to note that we also observed similar behavior in the AP sample regarding the abrupt increase of the width of the hyperfine field distribution. The AP sample does not show long range cooperative orbital ordering below T_c but our data reveals that short range orbital ordering may take place.

Figure 6 displays spectra taken in the presence of an external magnetic field of 60 kOe directed perpendicular to the propagation of γ -rays at selected temperatures. We notice that the spectrum at 4.2 K corresponds to a hyperfine field of 588 kOe which is larger by 60 kOe than the spectrum taken at zero external field. Furthermore the intensity of the absorption peaks are in the ratio of 3:4:1 indicating that the Fe magnetic moments are in the direction of the external magnetic field. The increase of the hyperfine field by 60 kOe on the other hand shows that

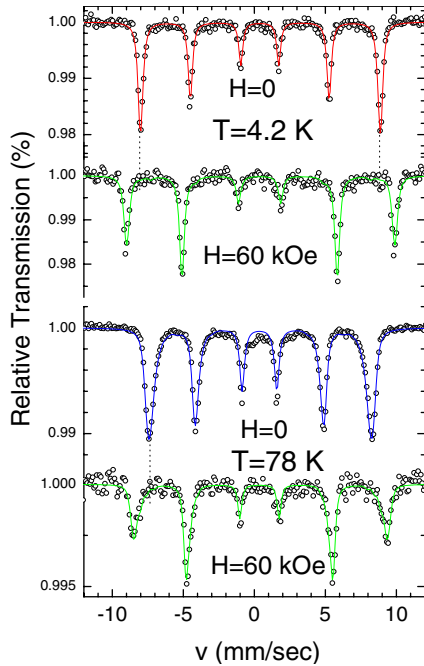


Fig. 6. Mössbauer spectra of R sample in the presence of an external magnetic field 60 kOe, at $T = 4.2$ K and 78 K. The external magnetic field is perpendicular to the γ -rays. The zero magnetic field spectra are also included in order to permit a direct comparison.

the electronic magnetic moment (due to the negative sign of the H_{hf}) are antiparallel to the external field. This can happen only if the Fe moments are antiferromagnetically coupled to the manganese moments (which in turn are parallel to the external field). A similar situation was encountered in the $x = 0.33$ system [13] while for the $x = 0.5$ system the Fe moment was ferromagnetically coupled to the Mn magnetic moments [14].

5 ESR and FMR results

Figure 7 shows representative ESR spectra for a powder AP sample as well as that of a small AP pellet, part of which was exposed to the maximum rf field to avoid excessive lineshape distortion due to the skin effect, at $T \leq 200$ K. An asymmetric ESR line is observed for both specimens, which broadens and shifts to lower fields as the FM ordering transition is approached, while a broad ferromagnetic resonance (FMR) mode is observed below T_c , and is sustained down to low temperatures. The resonance line can be effectively described by a linear superposition of absorption and dispersion components (Dysonian-like) including the tail of the resonance absorption at negative field, a consequence of the linearly polarized rf field which becomes important when the width is comparable to the resonance field. However, the specific resistivity $\rho = 1 - 2\Omega$ cm reported in the temperature range of 200–150 K, [19, 20, 24] yields skin depths of 0.52–0.73 mm at $\nu = 9.41$ GHz. These values being much larger than the average grain size of the powder specimen and comparable to that of the small bulk piece indicate that the persis-

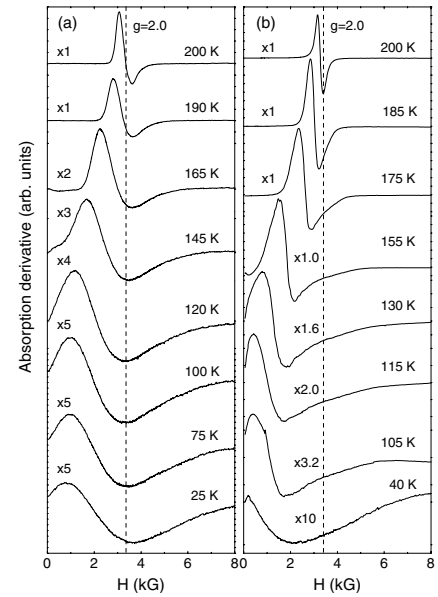


Fig. 7. Temperature dependence of the ESR spectra for (a) fine powder, and (b) pellet specimens of the (AP) sample at 9.41 GHz.

tent lineshape asymmetry, especially for the powder sample, is mainly determined by the distribution of the local anisotropy fields, frequently observed in the FMR spectra of polycrystalline ferromagnets [25–27] rather than by the reduced microwave penetration imposed by the skin effect.

Figure 8 shows the temperature dependence of the resonance field H_r and the linewidth ΔH for the powder and pellet (AP) specimens. A small shift of H_r is already seen at $T < 220$ K, above the T_c , similar to that observed in the paramagnetic regime of layered manganites, which has been explained by the contribution of demagnetizing fields as well as the presence of short-range anisotropic interactions [28]. At $T < 200$ K, a rapid shift of the FMR mode is observed down to $T \approx 130$ K, where a minimum of H_r is reached for the powder sample, followed by an almost linear increase down to low temperatures. This temperature variation agrees qualitatively with the expected increment of magnetic anisotropy in the FM phase, stemming from shape as well as magnetocrystalline anisotropy. Assuming a saturation magnetization of the order of $M_S = 3.5\mu_B/\text{Mn} \approx 550$ emu/cm³ for $x = 0.175$, a maximum demagnetizing field $4\pi M_S = 6.9$ kG is obtained. This may account for the shift of the FMR line when appropriately averaged for the crystallite shape distribution in a powder sample. This is further supported by the temperature dependence of the FMR line for the pellet specimen, where an enhanced shift of the FMR line due to demagnetizing fields is indeed observed (Fig. 7b). The linewidth goes through a minimum in the paramagnetic phase at $T_{\min} \approx 220$ K, and then increases considerably at lower temperatures. This is in agreement with previous ESR results suggesting inhomogeneous broadening induced by demagnetizing fields [29] rather than critical relaxation close to the FM transition [30]. However, a slower rate of the ΔH increment is observed below 150 K,

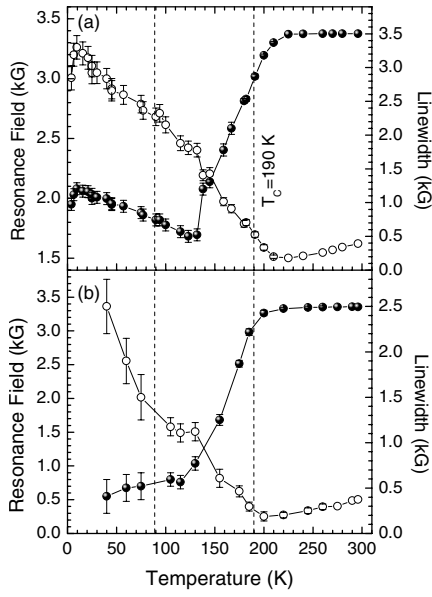


Fig. 8. Temperature dependence of the resonance field H_r and linewidth ΔH for (a) fine powder, and (b) pellet specimens of the (AP) sample.

followed by a more rapid increase at $T < 100$ K, for the pellet specimen.

Figure 9 shows typical ESR spectra observed for fine powdered R samples at different temperatures. A single ESR line at $g \approx 2.0$ is observed at $T > 200$ K in the paramagnetic regime, whereas a highly distorted FMR lineshape emerges at $T < T_c$, with the most pronounced distortion at $T < 75$ K, where the spectra appear to split into two broad modes. Complicated FMR spectra consisting of several narrow FMR lines have been reported for loose packed micron-sized powders ($5\text{--}20 \mu\text{m}$) obtained from crushed $\text{La}_{1-x}\text{Ca}_x\text{MnO}_3$ single crystals with $x = 0.18$ and 0.20 in the temperature range of $100\text{--}200$ K [19,31], whose convolution resemble the present broad FMR spectra at $T > 100$ K. These FMR lines have been found to shift excessively from the available field range upon lowering temperature, emphasizing the different grain morphology and the partial orientation effect along the easy magnetization axis that allow narrow lines to be identified, though with enhanced contribution of demagnetizing fields. To obtain an effective description of the FMR spectra, the lineshape was analyzed accordingly assuming the superposition of several resonance lines, each comprised of both absorption and dispersion components as well as the contribution of the resonance absorption at negative fields. A three-line pattern, one being centered near zero field, turned out to reproduce the FMR spectra in a relatively narrow temperature range below T_c ($160 < T < 190$ K), whereas a two-mode behavior at low (H_1) and high (H_2) magnetic fields with respect to $g = 2$, was found to adequately fit the FMR spectra at lower temperatures (Fig. 9). Alternatively, the average resonance field $H_{\text{ave}} = (H_R + H_L)/2$ and the peak-to-peak linewidth $\Delta H_{pp} = H_R - H_L$ were determined from the left and right spectrum peaks, which, however, disregard the

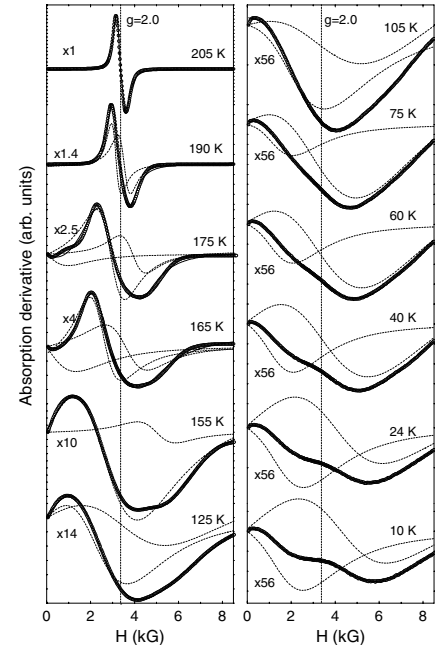


Fig. 9. Temperature dependence of the ESR spectra for a fine powder (R) sample at 9.41 GHz. Solid and dashed lines show the best-fit lineshapes of the total spectrum and its components, respectively.

spectrum structure, especially at the high field side of the resonance lineshape.

Figure 10 summarizes the temperature dependence of the resonance fields H_1 and H_2 and linewidths ΔH_1 and ΔH_2 as well as H_{ave} and ΔH_{pp} for the R sample. The third resonance line, which was identified at $160 \text{ K} < T < 190 \text{ K}$ was found to be centered at zero field $H_3 \sim 0$ with $\Delta H_3 = 1.8(1) \text{ kOe}$. A pronounced shift of the low-field component and a non-monotonous temperature variation of the high-field line can thus be observed (Fig. 10a). In particular, a maximum shift of H_2 at higher fields is attained at $T \approx 150$ K, followed by decreasing shifts at lower temperatures, while a reentrant increase of both resonance fields, more pronounced for the high-field component, is observed below 90 K. The corresponding linewidths increase rapidly upon lowering the temperature to $T \approx 150$ K, followed by a moderate increase down to 100 K, below which both lines narrow to an approximately constant value sustained down to the lowest temperatures (Fig. 10b). It is worth noting that the latter variations can hardly be distinguished in $H_{\text{ave}}(T)$ and $\Delta H_{pp}(T)$, which do not take into account the lineshape variations and resemble qualitatively the temperature dependence of FMR of the AP sample.

A distorted FMR lineshape can be, in principle, expected for random powders with high magnetocrystalline and shape anisotropy [25–27]. However, comparison with FMR data of the AP powder sample, which has similar grain morphology, implies an enhanced magnetocrystalline anisotropy for the R samples rather than a demagnetization effect. Angular dependent magnetization measurements of $\text{La}_{1-x}\text{Ca}_x\text{MnO}_3$ single crystal have shown the presence of uniaxial anisotropy of

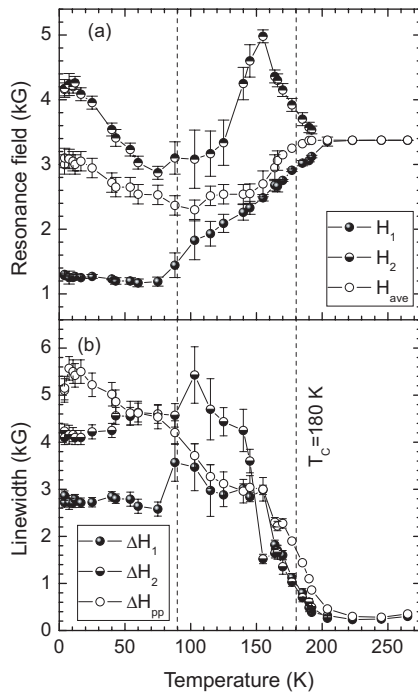


Fig. 10. Temperature dependence of the (a) resonance fields, and (b) linewidths of the (R) sample.

$K \approx 10^5$ erg/cm³ in the (110) plane for $x = 0.18$ [19], while significant rotation of the easy magnetization axis has been derived in the temperature range of 50–170 K for $x = 0.20$ [20]. The former value results in an anisotropy field $H_a = 2K/M_S = 360$ G, suggesting a sizeable contribution in the FMR spectra for the R samples. Based on the presence of strong non-uniaxial anisotropy, the two-component FMR spectra observed in crushed $\text{La}_{1-x}\text{Ca}_x\text{MnO}_3$ single crystals at $T > 100$ K were attributed to the FM insulating (FMI) phase, whereas the low-field FMR line detected in a relatively narrow temperature range below T_c was associated with the FM metallic phase (FMM) [19,31]. Even though our FMR data may be interpreted similarly at temperatures close to T_c , the excessive FMR broadening does not allow a reliable assessment of phase coexistence, as previously determined by thorough NMR investigations of low-doped $\text{La}_{1-x}\text{Ca}_x\text{MnO}_3$ [32,33]. On the other hand, the highly distorted FMR lineshape of the R samples suggest a relatively higher magnetic anisotropy with significant temperature dependence, in comparison with the AP samples. Relying on the temperature dependence of the two FMR components (Fig. 10) as reflected in the shift of spectral weight between the high and low-field sides of the total FMR spectrum (Fig. 9), an increase of the effective anisotropy can be inferred at $T \approx 150$ K, and most importantly a significant variation in the vicinity of 90 K, below which considerable increase is deduced. This would further correlate with the structural anomaly revealed by neutron scattering for $x > 0.125$ at $T < T_{O/O//}$, characterized by a strong decrease of orthorhombicity that signals a reentrance of the high-temperature pseudocubic phase [4], and also with recent NMR experiments

providing evidence for a transition to a collective state of FMI orbitally ordered domains separated by FMM walls [34]. Moreover, the latter effect should be relatively suppressed in the AP sample, in agreement with previous neutron diffraction investigations of AP samples with $x = 0.15$, showing the absence of any structural anomaly below T_c [35].

6 Conclusions

Our Mössbauer data reveal that the $\text{La}_{1-x}\text{Ca}_x\text{MnO}_3$ ($x = 0.175$) sample displays an anomaly in the temperature variation of the hyperfine field distribution of the probe ^{57}Fe nucleus which is related to supertransferred field. The change in the supertransferred field is closely connected with a new orbital transition at $T_{O/O//}$. Our recent neutron diffraction results revealed [6] that only the R samples display a structural anomaly at $T_{O/O//} = 100$ K. Furthermore, our Mössbauer spectra and magnetic measurements show this anomaly in both samples. This fact implies that the transition at $T_{O/O//}$ may be related to short range orbital rearrangement in the orbital “glass” for the AP sample, and coherent orbital rearrangement in the stoichiometric R sample. Since Mössbauer spectroscopy is a local probe it can detect changes that occur at the atomic level. The conclusions from the Mössbauer spectra can be further compared with the FMR data, which reveal significant differences between R and AP samples, implying an enhanced magnetic anisotropy with significant temperature variation in the former case. Most importantly, a pronounced variation of the effective anisotropy is inferred below $T_{O/O//}$ for the R samples, emphasizing the difference with the AP samples and supporting further the interpretation that in the latter class of materials the new orbital state is not of long-range character.

References

1. J.B. Goudenough, *Magnetism and Chemical Colossal Magnetoresistive Oxides*, edited by Y. Tokura (Gordon, Breach Science Publishers, 2000); *Colossal Magnetoresistance, Charge Ordering, Related Properties of Manganese Oxides*, edited by C.N. Rao, B. Raveau (World Scientific, 1998); *Physics of Manganites*, edited by T.A. Kaplan, S.D. Mahanti (Kluwer Academic/Plenum Publishers, 1999); N.R. Rao, A. Arulraj, A.K. Cheetham, B. Raveau, *J. Phys.: Condens. Mat.* **12**, R83 (2000); A.P. Ramirez, *J. Phys.: Condens. Mat.* **9**, 8171 (1997); Y. Tokura, Y. Tomioka, *J. Magn. Magn. Mater.* **200**, 1 (1999); J.M.D. Coey, M. Viret, S. von Molnar, *Adv. Phys.* **48**, 167 (1999); M.B. Salamon, M. Jaime, *Rev. Mod. Phys.* **73**, 583 (2001); E. Dagotto, T. Hotta, A. Moreo, *Phys. Rep.* **344**, 1 (2001); E.L. Nagaev, *Phys. Rep.* **346**, 387 (2001); A.J. Millis, *Nature* **392**, 147 (1998)
2. B. Dabrowski, R. Dybziński, Z. Bukowski, O. Chmaissem, *J. Solid State. Chem.* **146**, 448 (1999)
3. M. Pissas, G. Papavassiliou, *J. Phys.: Condens. Mat.* **16**, 6527 (2004)
4. G. Biotteau, M. Hennion, F. Moussa, J. Rodríguez-Carvajal, L. Pinsard, A. Revcolevschi, Y.M. Mukovskii, D. Shulyatev, *Phys. Rev. B* **64**, 104421 (2001)

5. S. Ishihara, S. Maekawa, Rep. Prog. Phys. **65**, 561 (2002) (references therein)
6. M. Pissas, I. Margiolaki, G. Papavassiliou, D. Stamopoulos, D. Argyriou, e-print: cond-matt, 0503253, in press, Phys. Rev. B (2005)
7. J. Geck, P. Wochner, D. Bruns, B. Büchner, U. Gebhardt, S. Kiele, P. Reutler, A. Revcolevschi, Phys. Rev. B **69**, 104413 (2004)
8. M. Pissas, G. Kallias, E. Devlin, A. Simopoulos, D. Niarchos, J. Appl. Phys. **81**, 8 (1997)
9. S.B. Ogale, R. Shreekala, R. Bathe, S.K. Date, S.I. Patil, B. Hannoyer, F. Petit, G. Marest, Phys. Rev. B **57**, 7841 (1998); B. Hannoyer, G. Marest, J.M. Greneche, R. Bathe, S.I. Patil, S.B. Ogale, Phys. Rev. B **61**, 9613 (2000)
10. A. Tkachuk, K. Rogacki, D.E. Brown, B. Dabrowski, A.J. Fedro, C.W. Kimball, B. Pyles, X. Xiong, Daniel Rosenmann, B.D. Dunlap, Phys. Rev. B **57**, 8509 (1998)
11. A. Simopoulos, G. Kallias, E. Devlin, I. Panagiotopoulos, M. Pissas, J. Magn. Magn. Mater. **177–181**, 860 (1998)
12. V. Chechersky, A. Nath, I. Isaac, J.P. Franck, K. Ghosh, H. Ju, R.L. Greene, Phys. Rev. B **59**, 497 (1999); V. Chechersky, A. Nath, I. Isaac, J.P. Franck, K. Ghosh, R.L. Greene, J. Phys.: Condens. Mat. **11**, 8921 (1999)
13. A. Simopoulos, M. Pissas, G. Kallias, E. Devlin, N. Moutis, I. Panagiotopoulos, D. Niarchos, C. Christides, R. Sonntag, Phys. Rev. B **59**, 1263 (1999)
14. G. Kallias, M. Pissas, E. Devlin, A. Simopoulos, D. Niarchos, Phys. Rev. B **59**, 1273 (1999)
15. G. Kallias, M. Pissas, E. Devlin, A. Simopoulos, Phys. Rev. B **65**, 144426 (2001)
16. A. Simopoulos, G. Kallias, E. Devlin, M. Pissas, Phys. Rev. B **63**, 054403 (2001)
17. P.A. Joy, S.K. Date, J. Magn. Magn. Mater. **220**, 106 (2000)
18. R. Laiho, E. Lähderanta, J. Salminen, K.G. Lisunov, V.S. Zakhvalinskii, Phys. Rev. B **63**, 094405 (2001)
19. V. Markovich, E. Rozenberg, A.I. Shames, G. Gorodetsky, I. Fita, K. Suzuki, R. Puzniak, D.A. Shulyatev, Y.M. Mukovskii, Phys. Rev. B **65**, 144402 (2002)
20. V. Markovich, I. Fita, R. Puzniak, M.I. Tsindlekht, A. Wisniewski, G. Gorodetsky, Phys. Rev. B **66**, 094409 (2002)
21. G. Le Caer, J.M. Dubois, J. Phys. E: Sci. Instrum. **12**, 1083 (1979)
22. *Effective field theories of magnetism*, J.E. Smart, W.B. Saunders Company, 1966
23. G.A. Sawatzky, F. Van der Woude, J. Phys. France **12**, C6-47 (1974)
24. T. Okuda, Y. Tomioka, A. Asamitsu, Y. Tokura, Phys. Rev. B **61**, 8009 (2000)
25. C.A. Morrison, N. Karayianis, J. Appl. Phys. **29**, 339 (1958)
26. E. Schlömann, J.R. Zeender, J. Appl. Phys. **29**, 341 (1958)
27. F.P. Valstyn, J.P. Hanton, A.H. Morrish, Phys. Rev. **128**, 2078 (1962)
28. N.O. Moreno, P.G. Pagliuso, C. Rettori, J.S. Gardner, J.L. Sarrao, J.D. Thompson, D.L. Huber, J.F. Mitchell, J.J. Martinez, S.B. Oseroff, Phys. Rev. B **63**, 174413 (2001)
29. F. Rivadulla, M.A. Lopez-Quintela, L.E. Hueso, J. Rivas, M.T. Causa, C. Ramos, R.D. Sanchez, M. Tovar, Phys. Rev. B **60**, 11 922 (1999)
30. V.A. Atsarkin, V.V. Demidov, F. Simon, R. Gaal, Y. Moritomo, K. Conder, A. Jánossy, L. Forró, J. Magn. Magn. Mater. **258–259**, 256 (2003)
31. A.I. Shames, E. Rozenberg, G. Gorodetsky, Ya.-M. Mukovskii, Phys. Rev. B **68**, 174402 (2003)
32. G. Papavassiliou, M. Belesi, M. Fardis, C. Dimitropoulos, Phys. Rev. Lett. **87**, 177204 (2001)
33. M. Belesi, G. Papavassiliou, M. Fardis, M. Pissas, J.E. Wegrowe, C. Dimitropoulos, Phys. Rev. B **63**, 180406 (2001)
34. G. Papavassiliou, M. Pissas, M. Belesi, M. Fardis, J. Dolinsek, C. Dimitropoulos, J.P. Ansermet, Phys. Rev. Lett. **91**, 147205 (2003)
35. Q. Huang, A. Santoro, J.W. Lynn, R.W. Erwin, J.A. Borchers, J.L. Peng, K. Ghosh, R.L. Greene, Phys. Rev. B **58**, 2684 (1998)